Journal of Physics: Photonics

OPEN ACCESS

RECEIVED
9 September 2021

REVISED
19 November 2021

ACCEPTED FOR PUBLICATION
8 December 2021

PUBLISHED
30 December 2021

PAPER

A generic model for the study of supercontinuum generation in graphene-covered nanowires

N Linale[1,4,*], P I Fierens[2,4], N Vermeulen[3] and D F Grosz[1,4]

[1] Departamento de Ingeniería en Telecomunicaciones, Centro Atómico Bariloche, Comisión Nacional de Energía Atómica, Río Negro 8400, Argentina
[2] Centro de Optoelectrónica, Instituto Tecnológico de Buenos Aires (ITBA), Ciudad Autónoma de Buenos Aires 1106, Argentina
[3] Brussels Photonics, Department of Applied Physics and Photonics, Vrije Universiteit Brussel, Pleinlaan 2, 1050 Brussel, Belgium
[4] Consejo Nacional de Investigaciones Científicas y Técnicas (CONICET), CABA C1425FQD, Argentina
* Author to whom any correspondence should be addressed.

E-mail: nicolas.linale@ib.edu.ar

Keywords: supercontinuum, generation, graphene, nanowires

Abstract

We study supercontinuum (SC) generation in graphene-covered nanowires based on a generic model that correctly accounts for the evolution of the photon number under Kerr and two-photon absorption processes, and the influence of graphene is treated within the framework of saturable photoexcited-carrier refraction. We discuss the role of the various effects on the generation of SC by a thorough analysis of short-pulse propagation in two different kinds of graphene-covered nanowires, one made of silicon nitride and the other made of silicon. Finally, we discuss the effect of stacking graphene layers as a means to enhance SC generation with pulse powers compatible with those in integrated optical devices.

1. Introduction

Supercontinuum (SC) generation is the subject of intense research in nonlinear optics [1–4], as it encounters applications in a vast number of areas in science and technology, such as in frequency combs [5, 6], spectroscopy, microscopy, and optical coherent tomography, among others [7].

Silicon nanowires have often been studied for SC generation as they exhibit large nonlinear coefficients (γ^{Kerr}) due to silicon's large nonlinear refractive index (n_2), two orders of magnitude larger than that of silica in the telecommunication band [8], and their small effective area (A_{eff}). Most importantly, they are compatible with CMOS fabrication [9] and have a wide transparency region in the near- and mid-infrared.

However, the large nonlinearity in silicon comes at the expense of two-photon absorption (TPA) [8] and free-carrier dispersion (FCD) and absorption (FCA) [10], phenomena that severely hinder the application of silicon nanowires in SC generation. Indeed, TPA and FCA/FCD have been shown to reduce the SC bandwidth and limit the maximum available power [2, 11, 12]. Silicon nitride (SiN), Si_3N_4, is an interesting alternative to silicon for nonlinear optical waveguides [13–15]. First, while SiN is also compatible with CMOS, it has a wider transparency window from 0.4 to $\sim$4 μm (see [15]), enabling its application to the visible spectrum [16]. Second, TPA is negligible in SiN at telecommunication wavelengths due to its much larger bandgap as compared to silicon [15, 17], a feature which has proved important in the design of microresonators and the generation of frequency combs and SC [18–21]. On the downside, the refractive index of SiN is $\sim$1.5 times smaller than that of silicon, leading to a reduced mode confinement, and its nonlinear refractive index is an order of magnitude smaller at telecom wavelengths [13].

When dealing with broad spectra as in SC generation, the frequency dependence of the nonlinear Kerr coefficient becomes of utmost importance. In particular, the effect of self-steepening (SS), related to the slope of the frequency dependence of γ^{Kerr}, comes into play [22, 23], as it is the case for silicon nanowires which exhibit frequency-dependent Kerr and TPA profiles [24]. It must be noted that this dependence is oftentimes modeled by the simple linear relation $\gamma(\Omega) = \gamma_0(1 + s\Omega/\omega_0)$, where Ω is the deviation from a central frequency ω_0 and s is the SS parameter. Furthermore, s is customarily set to unity due to the fact that

it is the only value which guarantees the conservation of the number of photons in the nonlinear Schrödinger equation (NLSE) [25]. However, silicon nanowires can have an arbitrary SS parameter [24, 26], and this poses a severe problem to the application of the NLSE in this scenario. For this reason, in [27] we introduced a new modeling equation, named the photon-conserving nonlinear Schrödinger equation (pcNLSE) which, based on a quantum-mechanical picture of the various nonlinear optical processes, guarantees strict conservation of the number of photons for any arbitrary frequency-dependent γ^{Kerr}. Moreover, the NLSE also exhibits problems when extended to include TPA by introducing a complex-valued nonlinear coefficient in straightforward fashion. Indeed, it can be shown that such an approach does not correctly model the cross-TPA of two co-propagating continuous waves, a fact that has led to the introduction of different modeling strategies. In particular, we extended the pcNLSE to account for TPA in [28]. We must emphasize that the pcNLSE and its modifications [29] have been successfully used to model the propagation of optical pulses in a variety of cases [30–34].

In the last few years, graphene has attracted great attention due to its singular electrical and optical properties [35–37]. In particular, it has been found that the magnitude of graphene's nonlinear refractive index is $\sim 10^6$–10^7 times that of silica [38, 39]. Interestingly, it has been shown that the nonlinear refractive index n_2 of quasi-undoped graphene is negative at telecommunication wavelengths [40]. This high nonlinearity can be advantageously used for SC generation and [41] shows SC generation in a silicon nanowire decorated with graphene. It must be noted that the integration of graphene on silicon devices has also been a subject of intense research in the last decade [42, 43].

There is a wide range of values for the nonlinear refractive index of graphene reported in the literature. In [44, 45] it is argued that this wide range stems from measurement conditions, such as the wavelength, duration and intensity of the propagated pulses. In particular, these references put forth an explanation for graphene's nonlinearity by means of saturable photoexcited-carrier refraction (SPCR). Not only SPCR accounts well for the values of n_2 reported in the literature [45], but it also allows to adequately model the nonlinear propagation of pulses in graphene-decorated waveguides [44].

In [44] the NLSE is modified to include SPCR in graphene. As we have already mentioned, the NLSE may lead to unphysical results in the case of broad spectra. For this reason and in order to study SC generation, in section 2, we incorporate SPCR into the pcNLSE. The new and generic modeling equation is validated in section 2.4 by comparing its predictions to experimental results in [44].

Although [44] reports an spectral broadening in a graphene-covered silica-core waveguide that is explained in terms of SPCR, no systematic analysis of all peculiarities of SC generation is carried out there. Therefore, the main goal of the present work is to complement [44] with such an analysis for the case of integrated devices covered with graphene. Note that this analysis does not include soliton dynamics as it is not of no relevance to the SPCR spectral-broadening mechanism. We base our study on the numerical investigation of two graphene-covered rectangular nanowires, one with a silicon core and another with a SiN core. In section 3 we present the main characteristics of these nanowires, where both have a rectangular core but different dimensions. Indeed, as we have already mentioned, SiN waveguides exhibit a reduced confinement as compared to silicon waveguides, which in turn affects quantitatively the SPCR phenomenon. Thus, we have designed the nanowires such that the effect of SPCR is similar in both cases. The role of SPCR in SC generation is studied in section 4. In particular, we demonstrate that SPCR-based SC spectra exhibit a unique behavior for shorter wavelengths, unlike that due to Kerr-generated SC. We also discuss the effect of stacking graphene layers to enhance SC generation. Finally, in section 5 we close with a summary and some final remarks.

2. Modeling framework

A complete modeling equation should take into account relevant effects in the waveguide and in the decorating material, namely linear absorption and dispersion, Kerr and TPA nonlinearities, FCA/FCD, and SPCR. Let us call $\tilde{A}_\Omega = \tilde{A}(z,\Omega) = \mathcal{F}(A_t)$ the Fourier transform of A_t, the complex envelope of the electric field normalized such that $|A_t|^2$ is the optical power. The propagation equation can then be written in the frequency domain as

$$\partial_z \tilde{A}_\Omega = -\frac{\alpha_{\text{eff}}}{2}\tilde{A}_\Omega + \hat{W}(\tilde{A}_\Omega, N_t^{\text{W}}) + \hat{G}(\tilde{A}_\Omega, N_t^{\text{G}}), \tag{1}$$

where we have grouped all intervening phenomena in three terms. The first term accounts for the linear loss, where α_{eff} is the effective loss coefficient calculated for the graphene-covered waveguide. The second term $\hat{W}$, which depends on the pulse envelope $\tilde{A}_\Omega$ and the free-carrier density in the core material of the waveguide N_t^{W}, accounts for the linear dispersion, the Kerr nonlinearity, FCA/FCD, and TPA in the core material.

Finally, the third term $\hat{G}$ depends on the photoexcited carrier density in graphene N_t^{G} and describes the contribution of the SPCR mechanism. We explain in detail each of these three terms in what follows.

2.1. Linear loss

The effective linear loss coefficient α_{eff} of the graphene-covered waveguide can be calculated as [46]

$$\alpha_{\mathrm{eff}} = \frac{\iint_{\mathrm{W}} \alpha(x,y)\,|F_\Omega(x,y)|^2\,dx\,dy}{\iint_{\mathrm{W}} |F_\Omega(x,y)|^2\,dx\,dy}, \tag{2}$$

where W is the cross-section of the waveguide, $\alpha(x,y)$ is the medium's loss, and $F_\Omega(x,y) = n(x,y)S_\Omega(x,y)$ is the mode distribution $S_\Omega(x,y)$ weighted by the refractive index $n(x,y)$. We do not include the effect of saturable absorption in graphene since it is not relevant for the low pulse energies considered in this work [17, 44].

2.2. Kerr, TPA and FCD/FCA

We have already presented an extension of the pcNLSE [27] that accounts for the Kerr and TPA effects in nanowires covered with 2D materials in [26]. We now complement that model with the inclusion of FCD and absorption phenomena taking place in the waveguide's core material. The complete model, corresponding to the $\hat{W}$ term in equation (1), reads

$$\begin{aligned}\hat{W} = {} & i\beta_\Omega \tilde{A}_\Omega + i\frac{(\omega_0+\Omega)r_\Omega}{2}\mathcal{F}\left(C_t^* B_t^2\right) + i\frac{(\omega_0+\Omega)r_\Omega^*}{2}\mathcal{F}\left(B_t^* C_t^2\right) \\ & - (\omega_0+\Omega)\eta_\Omega \mathcal{F}\left(|D_t|^2 D_t\right) - \frac{\sigma_{\mathrm{FC}}}{2}(1+i\mu_{\mathrm{FC}})\mathcal{F}\left[N_t^{\mathrm{W}} A_t\right],\end{aligned} \tag{3}$$

where ω_0 is the pump frequency, β_Ω is the dispersion profile, and r_Ω and η_Ω are related to the Kerr and TPA coefficients, respectively, through

$$r_\Omega = \sqrt[4]{\frac{\gamma_\Omega^{\mathrm{Kerr}}}{\omega_0+\Omega}}, \qquad \eta_\Omega = \sqrt[4]{\frac{\gamma_\Omega^{\mathrm{TPA}}}{\omega_0+\Omega}}. \tag{4}$$

γ^{Kerr} and γ^{TPA} are effective nonlinear coefficients which can be calculated as [26, 47]

$$\gamma_\Omega^{\mathrm{Kerr}} = \frac{(\omega_0+\Omega)}{c}\frac{\iint_{\mathrm{W}} n_2(x,y)\,|F_\Omega(x,y)|^4\,dx\,dy}{\left(\iint_{\mathrm{W}} |F_\Omega(x,y)|^2\,dx\,dy\right)^2}, \tag{5}$$

$$\gamma_\Omega^{\mathrm{TPA}} = \frac{(\omega_0+\Omega)}{2\omega_0}\frac{\iint_{\mathrm{W}} \beta^{\mathrm{TPA}}(x,y)\,|F_\Omega(x,y)|^4\,dx\,dy}{\left(\iint_{\mathrm{W}} |F_\Omega(x,y)|^2\,dx\,dy\right)^2}, \tag{6}$$

where n_2 and β^{TPA} are the nonlinear refractive index and the TPA coefficient, respectively, and c is the speed of light. It must be noted that we do not include the effect of graphene in these equations as its nonlinear behavior is modeled by the SPCR mechanism. The fields B_t, C_t, and D_t are defined in the frequency domain by

$$\tilde{B}_\Omega = r_\Omega \tilde{A}_\Omega, \qquad \tilde{C}_\Omega = r_\Omega^* \tilde{A}_\Omega, \qquad \tilde{D}_\Omega = \eta_\Omega \tilde{A}_\Omega. \tag{7}$$

The last term in equation (3) models FCD and absorption, following the well established approach in the literature. We introduce coefficients σ_{FC} and μ_{FC} which account for FCA and FCD in the waveguide's core material, respectively, and the evolution of the free-carrier density in the waveguide's core, N_t^{W}, is calculated as [46, 48]

$$\partial_t N_t^{\mathrm{W}} = \frac{\gamma^{\mathrm{TPA}}}{\hbar\omega_0 A_{\mathrm{eff}}}|A_t|^4 - \frac{N_t^{\mathrm{W}}}{\tau_{\mathrm{c}}^{\mathrm{W}}}, \tag{8}$$

where A_{eff} is the effective mode area at the pump wavelength and $\tau_{\mathrm{c}}^{\mathrm{W}}$ is the effective carrier lifetime.

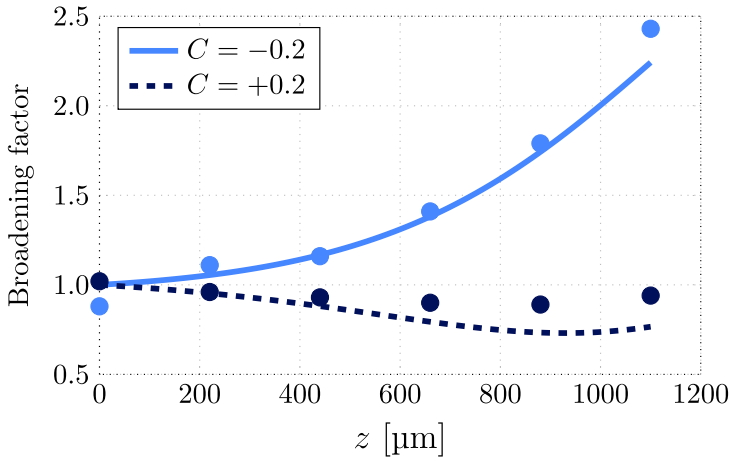

Figure 1. Validation of the proposed model with experimental data (circles) in [44], where a 2.7 W, 3 ps chirped sech pulse propagates in a waveguide decorated with a single graphene layer. The waveguide is made of a SiO_2 core region (500 nm thick) sandwiched between two horizontal SiN stripes (170 nm thick). (Solid line) $C = -0.2$ and (dashed line) $C = +0.2$.

2.3. Saturable photoexcited-carrier absorption

Following [44], we model FCD due to the graphene layers, as

$$\hat{G} = i\sigma_{\mathrm{SP}}\mathcal{F}\left[N_t^{\mathrm{G}} A_t\right], \tag{9}$$

where the coefficient σ_{SP} is wavelength dependent. Due to Pauli blocking, the photoexcited carrier density resulting from graphene's linear absorption can saturate. Indeed, the temporal evolution of the carrier density is given by [44]

$$\partial_t N_t^{\mathrm{G}} = \frac{\alpha_{\mathrm{eff}}(0)}{\hbar\omega_0}\left[1 - \frac{N_t^{\mathrm{G}}}{N_{\mathrm{sat}}}\right]|A_t|^2 - \frac{N_t^{\mathrm{G}}}{\tau_{\mathrm{c}}^{\mathrm{G}}}, \tag{10}$$

where N_{sat} is the saturation parameter, and $\tau_{\mathrm{c}}^{\mathrm{G}}$ is the effective carrier lifetime of the graphene-covered waveguide and $\alpha_{\mathrm{eff}}(0)$ is the effective linear loss at the pump wavelength. Observe that N_t^{G} is a linear density due to the 2D nature of graphene, in contrast to N_t^{W} which is a volume density. The SPCR coefficient can be calculated as [45]

$$\sigma_{\mathrm{SP}} = -\frac{\pi\alpha}{2\, n_{\mathrm{eff}}}\frac{\mathrm{Im}\left\{\Delta\sigma^{(1)}/\sigma_0\right\}}{N_{\mathrm{sat}}/2}\frac{\int_{\mathrm{G_x}}|F_\Omega(x, y_{\mathrm{G}})|^2\, dx}{\iint_{\mathrm{W}}|F_\Omega(x,y)|^2\, dx\, dy}, \tag{11}$$

where $\alpha \approx 1/137$ is the fine-structure constant, $\Delta\sigma^{(1)} = \sigma^{(1)}(N_{\mathrm{sat}}/2) - \sigma^{(1)}(0)$, $\sigma^{(1)}$ is the conductivity of graphene, $\sigma_0 = e^2/4\hbar$ is the universal conductivity, and n_{eff} is the effective mode index. Castelló-Lurbe *et al* [45] presents details of the calculation of $\sigma^{(1)}$ as a function of the carrier density, as well as a derivation of equation (10), modeling the evolution of photoexcited carriers, on the basis of the theoretical model in [49, 50]. The two-dimensional graphene layers are assumed to be on a line segment $\mathrm{G_x}$. It must be noted that we not only consider dependence on frequency of the mode distribution, but also that of graphene's conductivity.

2.4. Model validation

We validate our modeling framework by comparing results from equation (1) with experimental results from [44]. Although the details of the waveguide can be found in that work, let us note that it consists of a SiO_2 core region sandwiched by two narrow SiN stripes, covered with a single layer of graphene on top, and with a length of up to 1100 μm.

We launched two 2.7 W, 3 ps (FWHM) sech pulses at $\lambda_0 = 1563$ nm, one with a positive chirp $C = +0.2$ and another with a negative chirp $C = -0.2$. We measured the broadening factor as $\mu_2(L)/\mu_2(0)$, where L is the waveguide length and $\mu_2(z) = (\int_{-\infty}^{+\infty}|\partial_t A_t|^2 dt)/(\int_{-\infty}^{+\infty}|A_t|^2 dt)$. Figure 1 shows the results for both pulses, exhibiting a good agreement between our simulations and the experimental results in [44].

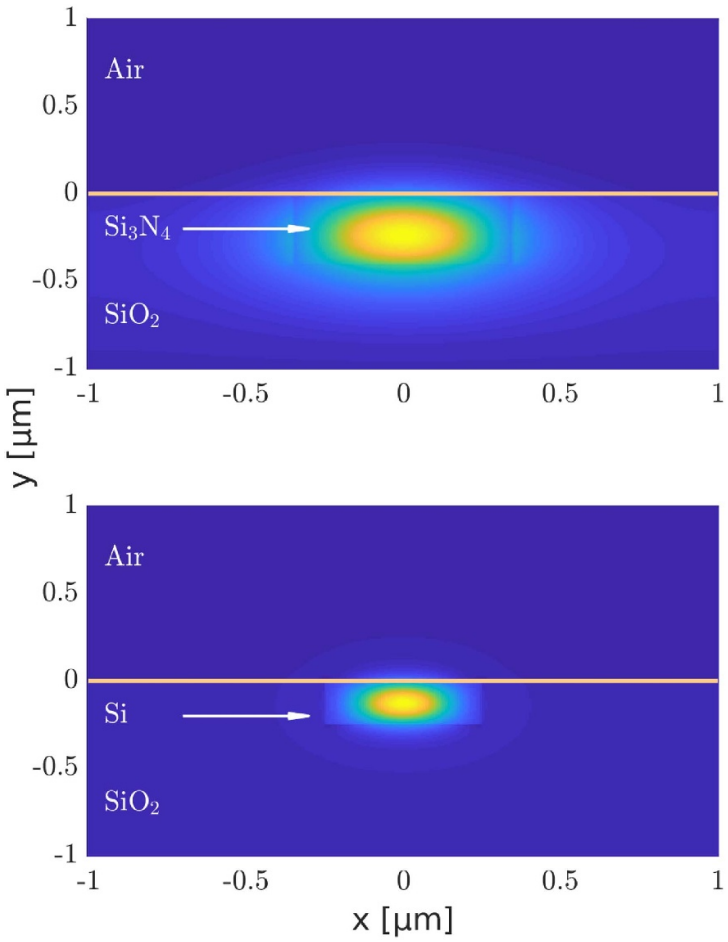

Figure 2. Cross section and transverse-electric mode distribution at $\lambda_0 = 1550$ nm for graphene-covered 700 × 400 nm SiN (top) and 500 × 250 nm silicon (bottom) waveguides. Despite the different cross sections both waveguides have similar SPCR coefficients. Yellow lines represent graphene layers.

3. Choice of waveguide material and dimensions

In order to analyze the role of SPCR in SC generation, we study the propagation of short pulses at $\lambda_0 = 1550$ nm in two graphene-covered nanowires buried in a silica (SiO_2) substrate. We use two different materials for the core, silicon and SiN, as they are both relevant for integrated photonic devices and have different optical characteristics as explained in section 1. The cross-section of the SiN waveguide is 700 × 400 nm, while that of the silicon waveguide is 500 × 250 nm. We choose different dimensions in order to obtain similar values of the SPCR coefficient σ_{SP} (see figure 4), and we vary the number of graphene layers in order to study its influence. We consider modest doping of graphene with a hole density of $p_0 = 6.5 \times 10^{12}$ cm^{-2} as in [44, 45]. Figure 2 shows the cross-section of the graphene-covered SiN (top) and silicon (bottom) waveguides and the transverse-electric mode distribution, computed by means of a finite-difference time-domain (FDTD) algorithm [52].

A careful analysis of equation (1) reveals that, in order to take full advantage of graphene for SC generation, the term $\hat{G}$ must be increased. According to equation (9), this can be achieved by either increasing $|\sigma_{SP}|$ or N_{sat}. Even though both σ_{SP} and N_{sat} are not independent as they are related through equation (11), there is a straightforward way of increasing both simultaneously, i.e. by increasing the number of graphene layers. Figure 3 shows that both N_{sat}^2 and the imaginary part of $\Delta\sigma^{(1)}/\sigma_0$ increase with the number of layers (N_{sat} was taken from [51] and $\sigma^{(1)}$ in this figure is calculated at 1550 nm as in [45]). Although $\Delta\sigma^{(1)}$ is divided by N_{sat} in equation (11), the net effect of their variation is to increase $|\sigma_{SP}|$ with the number of layers. This can be observed in figure 4 where the wavelength-dependent coefficients for the SiN (top) and Si nanowire (bottom), and for 1, 2 and 4 decorating layers are shown. It can be readily seen that $|\sigma_{SP}|$ rapidly increases with wavelength, a fact correlated with the mode confinement.

The frequency-dependent dispersion, Kerr, and TPA profiles for the waveguide's core material were calculated using equations (5), (6) and the mode distribution, obtained by means of an FDTD algorithm, and are shown in figure 5. The remaining waveguide parameters are taken from the literature and are shown

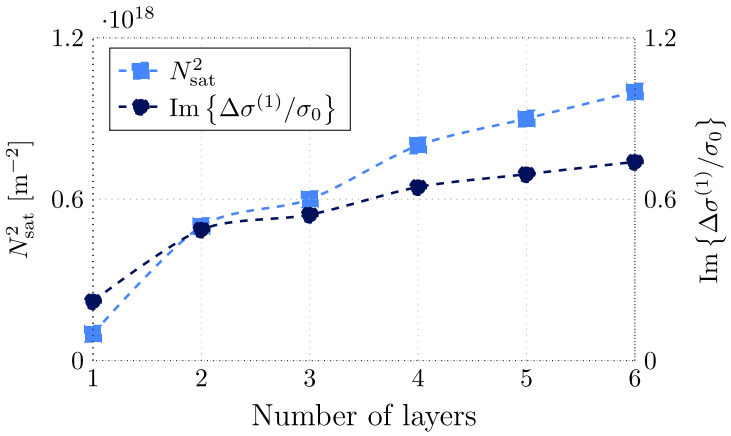

Figure 3. Saturation parameter, N_{sat}^2, and imaginary part of the normalized conductivity of graphene, $\text{Im}\{\Delta\sigma^{(1)}/\sigma_0\}$, as a function of the number of decorating layers for $\lambda = 1550$ nm. N_{sat} taken from [51]. $\Delta\sigma^{(1)}$ was calculated as in [45], setting the initial hole density to $p_0 = 6.5 \times 10^{12}$ cm^{-2}, and the scattering parameters for intra- and interband transitions to $\Gamma_{intra} = \Gamma_{inter} = 33$ meV.

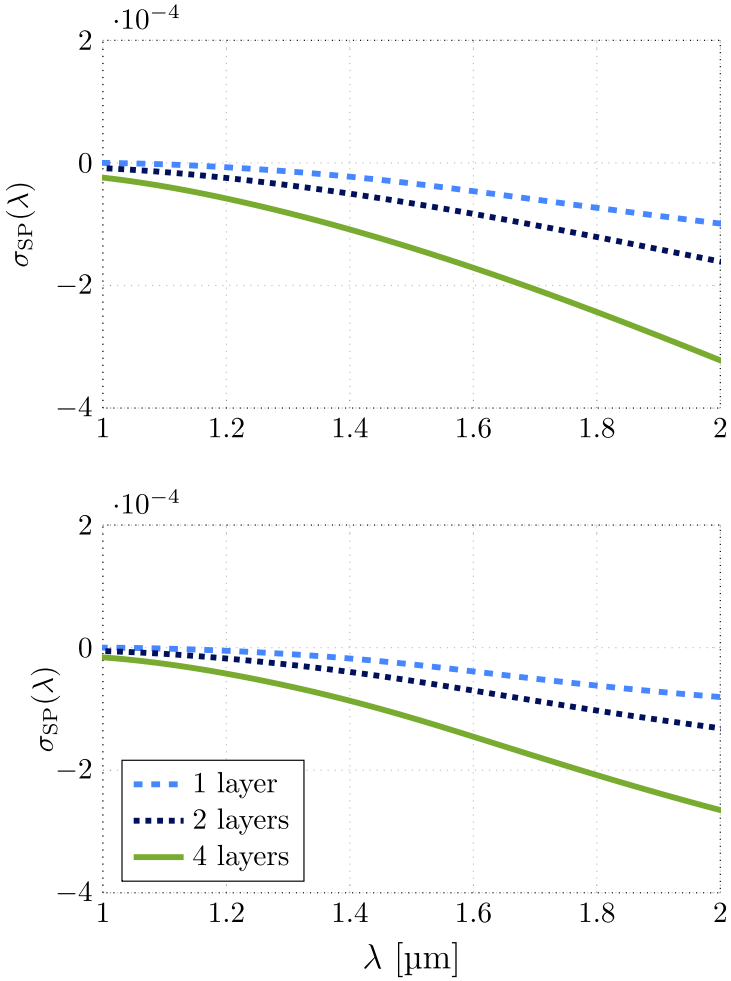

Figure 4. Wavelength dependence of the SPCR coefficient, σ_{SP}, for the 700 × 400 nm SiN (top) and the 500 × 250 nm silicon waveguide (bottom), covered with 1 (dashed), 2 (dotted), and 4 (solid) graphene layers. Note that despite the different cross sections both waveguides exhibit similar SPCR coefficients.

for reference in table 1. Note that the frequency dependence of the effective linear loss was not taken into account as we verified that it has a negligible effect on simulation results. Furthermore, TPA is not relevant at low optical powers and, for the sake of simplicity, in equation (8) we assumed a frequency-independent A_{eff} equal to the cross-section area of the core waveguide.

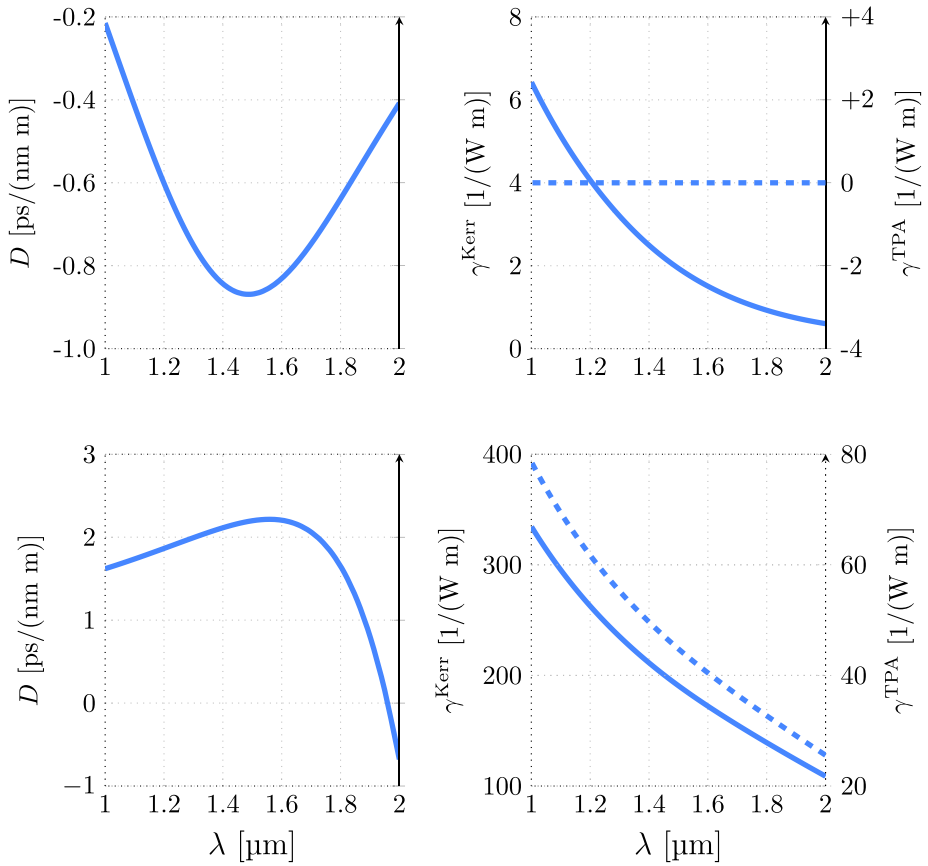

Figure 5. Wavelength dependence of the dispersion (left) and the Kerr (right, solid line) and TPA (right, dashed line) coefficients for the 700 × 400 nm SiN (top) and the 500 × 250 nm silicon waveguide (bottom).

Table 1. Simulation parameters.

Waveguide	Si_3N_4	Si
Effective absorption[a], α_{eff} (μm^{-1})		
Bare	7.0×10^{-6}	7.7×10^{-7}
1 layer	8.0×10^{-3}	1.2×10^{-2}
2 layers	1.5×10^{-2}	2.5×10^{-2}
N^2_{sat} (m^{-2})[b]		
1 layer	1×10^{17}	
2 layers	5×10^{17}	
Graphene parameters		
τ_c^G (ps)[c]	1	200
$\sigma_{SP}(\lambda)$	Shown in figure 4	
FCA/FCD[d]		
σ_{FC} (m^2)	—	1.45×10^{-21}
μ_{FC}	—	7.55
τ_c^W (ps)	—	200

[a] Calculated as in equation (2), using information from [51, 53, 54].
[b] See figure 3.
[c] Taken from [44].
[d] Taken from [11].

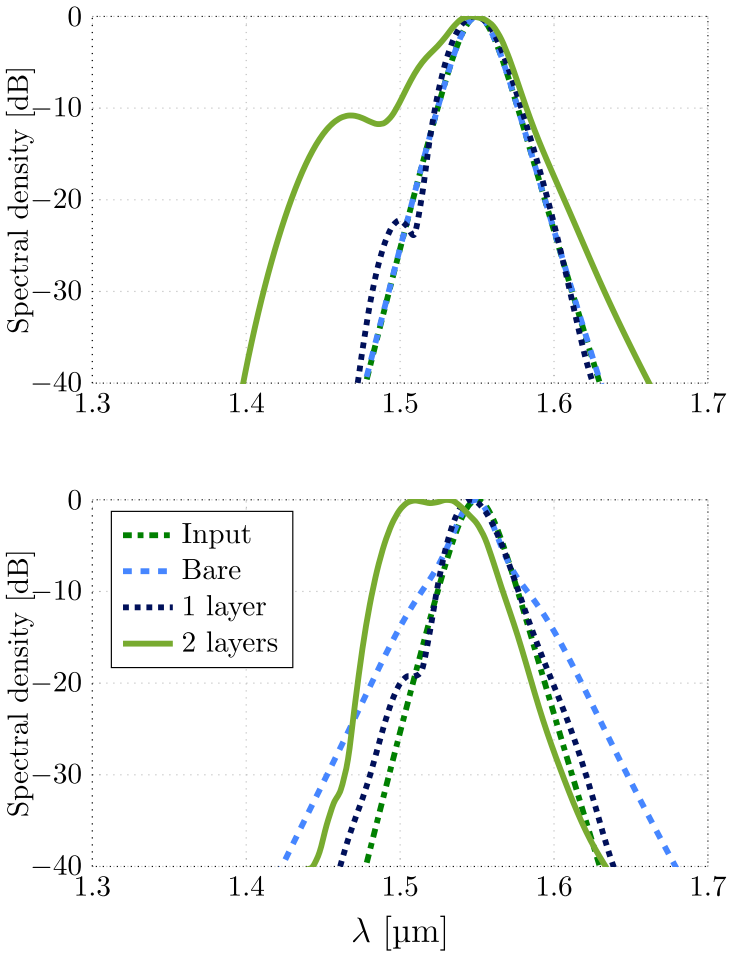

Figure 6. Influence of the number of graphene layers on SC for the SiN (top) and silicon (bottom) waveguides. Input normalized spectral density (dashed-dotted) and output of bare (dashed), and covered waveguides with one (dotted) and two graphene layers (solid).

4. Simulation results and discussion

In order to study the influence of the number of graphene layers, we performed simulations on both silicon and SiN 300 μm long waveguides, covered with one or two graphene layers, and launching a 45 W 100 fs (FWHM) transform-limited sech pulse at $\lambda_0 = 1550$ nm. Results are shown in figure 6 where, for the sake of comparison, we also include the output spectrum of the bare waveguide. It can be readily observed that the output spectrum in the bare SiN waveguide (top) is almost identical to that at the input, i.e. there is no spectral broadening. However, in both waveguides the output spectrum broadens as more graphene layers are added. It is worth noting that SPCR distinctively manifests itself by increasing the bandwidth on the blue side of the spectrum. We verified that the narrower output spectrum in the silicon waveguide is a consequence of the combined effects of linear loss and chromatic dispersion. Blueshifting of short pulses was first theoretically proposed by Serkin and Visloukh [55], and it was theoretically and experimentally studied in gas-filled photonic crystal fibers [56, 57] and silicon waveguides [11, 58, 59]. More interestingly, it has been observed in the response of graphene to ultrafast optical fields [50].

The relation between photoexcited-carrier dynamics and the spectral blueshift has been previously reported in [50]. As such, it is interesting to look at their dynamics in our examples. This is displayed in figure 7 where the temporal evolution of the photoexcited-carrier density at the output of the Si and SiN waveguides, both covered with two graphene layers, are shown. As the carrier effective recombination time in the silicon waveguide is much longer than the pulse duration (see table 1), the carrier density presents a step-like characteristic; however, a different behavior is observed in the SiN waveguide due to the much shorter recombination time. In both cases, there is a fast rise time for the carrier build-up and as such a fast carrier-induced change in refractive index. These results are consistent with those reported in [44]. Also, note that the carrier density does not reach saturation at the output of the Si waveguide, due to the large power loss, as it does in the SiN case.

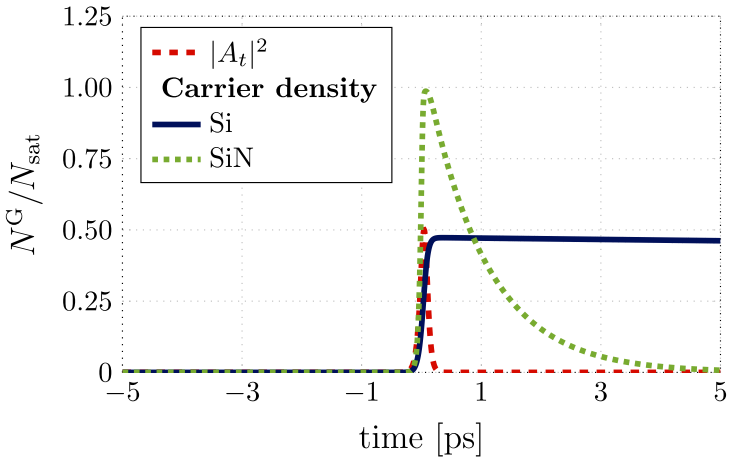

Figure 7. Normalized carrier density at the output end of the silicon waveguide (blue solid line) and the SiN waveguide (green dotted line), covered with two graphene layers, for a 45 W input pulse. The pulse envelope (red dashed line) is shown for the sake of reference (arbitrary units). Results include all nonlinear effects.

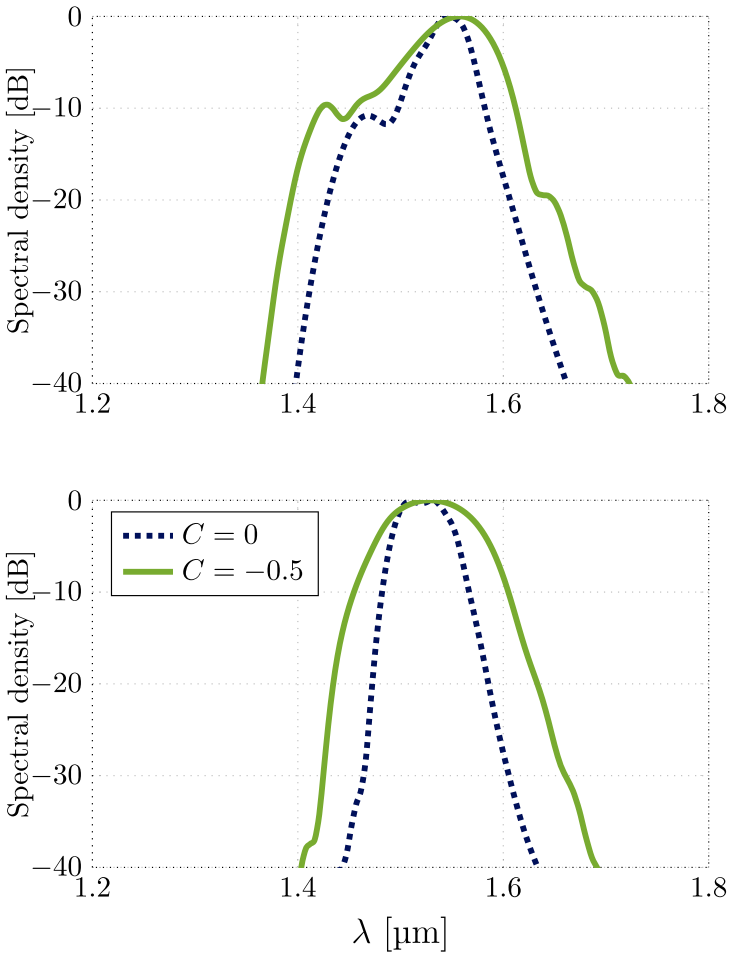

Figure 8. Effect of negative chirp on SC for the SiN (top) and silicon waveguide (bottom) covered with two graphene layers. Output normalized spectral density for input chirps $C = 0$ (dotted) and $C = -0.5$ (solid).

Experimental results in [44] suggest that a negative-chirped input pulse may lead to a broader output spectrum. Figure 8 shows numerical results (same input parameters as in figure 6) for two graphene layers, where a negative chirping factor $C = -0.5$ (solid line) was set. For the sake of comparison, the output for a chirpless input pulse with $C = 0$ (dotted line) is also plotted. Top and bottom panels show the SiN and Si nanowires, respectively. The effect of pre-chirping is seen to be beneficial in terms of increasing the SC bandwidth on the red side of the spectrum for both waveguide core materials.

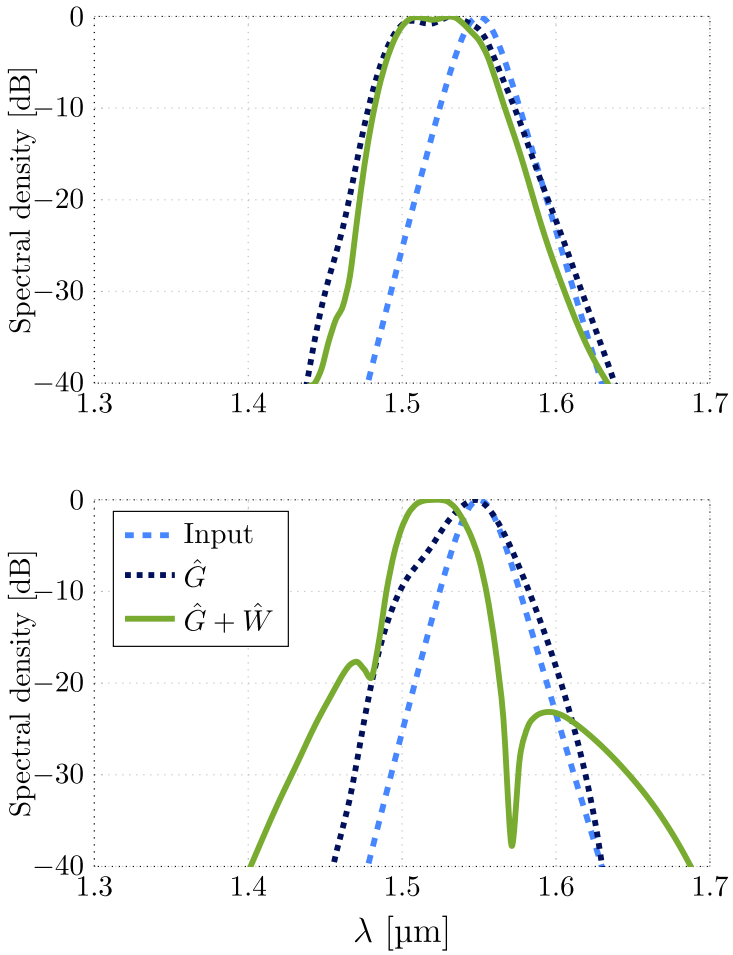

Figure 9. Influence of γ^{Kerr}, γ^{TPA}, and FCD/FCA for the silicon waveguide covered with two graphene layers, and for a 45 W (top) and a 500 W input (bottom). Input normalized spectral density (dashed) and output spectra considering only SPCR (dotted) and all effects combined (solid).

Results in figure 6 suggest that the power level might not be high enough to excite Kerr, TPA, and free-carrier contributions in the silicon waveguide. As such, we explore these effects at higher power levels in the silicon waveguide covered with two graphene layers. Figure 9 shows results for a 45 W (top) and a 500 W input (bottom), separating the aforementioned effects from the SPCR mechanism. Spectral broadening due to SPCR is similar for both input powers, signaling that at a higher input power the SPCR contribution is fully saturated (see [44]). Further spectral broadening for the 500 W input is driven by Kerr (and limited by FCA/FCD and TPA) in the core material of the waveguide.

5. Conclusions

The large optical nonlinearity of graphene has brought about considerable interest for its potential use in integrated photonics, where a particular application of singular relevance is that of SC generation. In spite of the large volume of literature on the subject, still there is discussion on the physical mechanisms leading to such large nonlinearity. SPCR has recently been proposed as an adequate explanation in good agreement with experimental results.

In this work, we focus on the study of the role of SPCR in SC generation in graphene-covered nanowires by means of an extended model. This generic approach takes into account the effect of graphene by means of SPCR and all other relevant nonlinear phenomena in the underlying core waveguide within the framework of a photon-conserving (in the absence of loss mechanisms) modeling equation. Further, we explored SC generation with pulse powers compatible with those in integrated photonic devices. We showed that a distinct signature of the SPCR mechanism is the blueshifting of the output SC spectrum, an observation that has been already reported in [11]. The influence of the number of graphene layers on SC generation was also analyzed, finding that the resulting spectrum broadens as the number of layers increases from one to two. Moreover, we showed that this is related to the increment of the SPCR coefficient (in absolute value) and the

saturation parameter with the number of layers. Finally, we showed that negatively-chirped input pulses contribute to a broader SC, in accordance with previous experimental observations of SPCR in graphene-covered nanowires, albeit at more modest spectral broadenings. We believe results in this work help reveal and optimize the contributions from the various nonlinear phenomena leading to SC generation in graphene-covered integrated optics, thus putting forth a useful modeling tool for the design of devices and their characterization.

Data availability statement

All data that support the findings of this study are included within the article (and any supplementary files).

Acknowledgments

Nathalie Vermeulen acknowledges partial financial support by Fonds Wetenschappelijk Onderzoek (FWO) under Grants G005420N and G0F6218N (EOS-convention 30467715), and by VUB-OZR.

ORCID iDs

N Linale https://orcid.org/0000-0003-3508-7903
P I Fierens https://orcid.org/0000-0001-5725-0017
N Vermeulen https://orcid.org/0000-0001-9676-0095

References

[1] Dudley J M, Genty G and Coen S 2006 Supercontinuum generation in photonic crystal fiber *Rev. Mod. Phys.* **78** 1135
[2] Hsieh I-W *et al* 2007 Supercontinuum generation in silicon photonic wires *Opt. Express* **15** 15242–9
[3] Singh N *et al* 2015 Midinfrared supercontinuum generation from 2 to 6 μm in a silicon nanowire *Optica* **2** 797–802
[4] Singh N *et al* 2018 Octave-spanning coherent supercontinuum generation in silicon on insulator from 1.06 μm to beyond 2.4 μm *Light Sci. Appl.* **7** 17131
[5] Pfeifle J *et al* 2014 Coherent terabit communications with microresonator Kerr frequency combs *Nat. Photon.* **8** 375–80
[6] Griffith A G *et al* 2015 Silicon-chip mid-infrared frequency comb generation *Nat. Commun.* **6** 6299
[7] Nishizawa N 2012 Generation and application of high-quality supercontinuum sources *Opt. Fiber Technol.* **18** 394–402
[8] Dinu M, Quochi F and Garcia H 2003 Third-order nonlinearities in silicon at telecom wavelengths *Appl. Phys. Lett.* **82** 2954–6
[9] Kuyken B *et al* 2015 An octave-spanning mid-infrared frequency comb generated in a silicon nanophotonic wire waveguide *Nat. Commun.* **6** 1–6
[10] Soref R A and Bennett B R 1987 Electrooptical effects in silicon *IEEE J. Quantum Electron.* **23** 123–9
[11] Yin L and Agrawal G P 2007 Impact of two-photon absorption on self-phase modulation in silicon waveguides *Opt. Lett.* **32** 2031–3
[12] Yin L, Lin Q and Agrawal G P 2007 Soliton fission and supercontinuum generation in silicon waveguides *Opt. Lett.* **32** 391–3
[13] Moss D J, Morandotti R, Gaeta A L and Lipson M 2013 New CMOS-compatible platforms based on silicon nitride and hydex for nonlinear optics *Nat. Photon.* **7** 597–607
[14] Baets R *et al* 2016 Silicon photonics: silicon nitride versus silicon-on-insulator *Optical Fiber Communication Conf.* (Optical Society of America) p Th3J.1
[15] Rahim A *et al* 2017 Expanding the silicon photonics portfolio with silicon nitride photonic integrated circuits *J. Lightwave Technol.* **35** 639–49
[16] Romero-García S, Merget F, Zhong F, Finkelstein H and Witzens J 2013 Silicon nitride CMOS-compatible platform for integrated photonics applications at visible wavelengths *Opt. Express* **21** 14036–46
[17] Demongodin P *et al* 2019 Ultrafast saturable absorption dynamics in hybrid graphene/Si_3N_4 waveguides *APL Photonics* **4** 076102
[18] Okawachi Y, Saha K, Levy J S, Wen Y H, Lipson M and Gaeta A L 2011 Octave-spanning frequency comb generation in a silicon nitride chip *Opt. Lett.* **36** 3398–400
[19] Liu Y *et al* 2014 Investigation of mode coupling in normal-dispersion silicon nitride microresonators for Kerr frequency comb generation *Optica* **1** 137–44
[20] Pfeiffer M H, Kordts A, Brasch V, Zervas M, Geiselmann M, Jost J D and Kippenberg T J 2016 Photonic damascene process for integrated high-Q microresonator based nonlinear photonics *Optica* **3** 20–25
[21] El Dirani H *et al* 2018 Annealing-free Si_3N_4 frequency combs for monolithic integration with Si photonics *Appl. Phys. Lett.* **113** 081102
[22] Kibler B, Dudley J M and Coen S 2005 Supercontinuum generation and nonlinear pulse propagation in photonic crystal fiber: influence of the frequency-dependent effective mode area *Appl. Phys.* B **81** 337–42
[23] Gaafar M A, Baba T, Eich M and Petrov A Y 2019 Front-induced transitions *Nat. Photon.* **13** 737–48
[24] Panoiu N C, Liu X and Osgood R M Jr 2009 Self-steepening of ultrashort pulses in silicon photonic nanowires *Opt. Lett.* **34** 947–9
[25] Blow K J and Wood D 1989 Theoretical description of transient stimulated Raman scattering in optical fibers *IEEE J. Quantum Electron.* **25** 2665–73
[26] Linale N, Bonetti J, Sánchez A D, Fierens P I and Grosz D F 2021 Model for frequency-dependent nonlinear propagation in 2D-decorated nanowires *IEEE J. Quantum Electron.* **57** 6100308
[27] Bonetti J, Linale N, Sánchez A D, Hernandez S M, Fierens P I and Grosz D F 2019 Modified nonlinear Schrödinger equation for frequency-dependent nonlinear profiles of arbitrary sign *J. Opt. Soc. Am.* B **36** 3139–44
[28] Linale N, Bonetti J, Sparapani A, Sánchez A D and Grosz D F 2020 Equation for modeling two-photon absorption in nonlinear waveguides *J. Opt. Soc. Am.* B **37** 1906–10

[29] Bonetti J, Linale N, Sánchez A D, Hernandez S M, Fierens P I and Grosz D F 2020 Photon-conserving generalized nonlinear Schrödinger equation for frequency-dependent nonlinearities *J. Opt. Soc. Am.* B **37** 445–50
[30] Linale N, Bonetti J, Sánchez A D, Hernandez S, Fierens P I and Grosz D F 2020 Modulation instability in waveguides with an arbitrary frequency-dependent nonlinear coefficient *Opt. Lett.* **45** 2498–501
[31] Sánchez A D, Linale N, Bonetti J and Grosz D F 2020 Modulation instability in waveguides doped with anisotropic nanoparticles *Opt. Lett.* **45** 3119–22
[32] Linale N, Fierens P I, Bonetti J, Sánchez A D, Hernandez S M and Grosz D F 2020 Measuring self-steepening with the photon-conserving nonlinear Schrödinger equation *Opt. Lett.* **45** 4535–8
[33] Linale N, Bonetti J, Fierens P I, Hernandez S M and Grosz D F 2021 A direct method for the simultaneous estimation of self-steepening and the fractional Raman contribution in fiber optics *IEEE J. Quantum Electron.* **57** 6800207
[34] Sánchez A D, Linale N and Grosz D F 2021 Simple model for the nonlinear optical response of dimer-doped waveguides *J. Opt. Soc. Am.* B **38** 17–23
[35] Cao M-S, Wang X-X, Cao W-Q and Yuan J 2015 Ultrathin graphene: electrical properties and highly efficient electromagnetic interference shielding *J. Mater. Chem.* C **3** 6589–99
[36] Hafez H A, Kovalev S, Tielrooij K-J, Bonn M, Gensch M and Turchinovich D 2020 Terahertz nonlinear optics of graphene: from saturable absorption to high-harmonics generation *Adv. Opt. Mater.* **8** 1900771
[37] Romagnoli M *et al* 2018 Graphene-based integrated photonics for next-generation datacom and telecom *Nat. Rev. Mater.* **3** 392–414
[38] Chen W *et al* 2013 The nonlinear optical properties of coupling and decoupling graphene layers *AIP Adv.* **3** 042123
[39] Demetriou G, Bookey H T, Biancalana F, Abraham E, Wang Y, Ji W and Kar A K 2016 Nonlinear optical properties of multilayer graphene in the infrared *Opt. Express* **24** 13033–43
[40] Vermeulen N, Castelló-Lurbe D, Cheng J, Pasternak I, Krajewska A, Ciuk T, Strupinski W, Thienpont H and Van Erps J 2016 Negative Kerr nonlinearity of graphene as seen via chirped-pulse-pumped self-phase modulation *Phys. Rev. Appl.* **6** 044006
[41] Ishizawa A *et al* 2017 Optical nonlinearity enhancement with graphene-decorated silicon waveguides *Sci. Rep.* **7** 45520
[42] Kim K, Choi J-Y, Kim T, Cho S-H and Chung H-J 2011 A role for graphene in silicon-based semiconductor devices *Nature* **479** 338–44
[43] Akinwande D, Huyghebaert C, Wang C-H, Serna M I, Goossens S, Li L-J, Wong H-S P and Koppens F H 2019 Graphene and two-dimensional materials for silicon technology *Nature* **573** 507–18
[44] Vermeulen N *et al* 2018 Graphene's nonlinear-optical physics revealed through exponentially growing self-phase modulation *Nat. Commun.* **9** 1–9
[45] Castelló-Lurbe D, Thienpont H and Vermeulen N 2020 Predicting graphene's nonlinear-optical refractive response for propagating pulses *Laser Photonics Rev.* **14** 1900402
[46] Lin Q, Painter O J and Agrawal G P 2007 Nonlinear optical phenomena in silicon waveguides: modeling and applications *Opt. Express* **15** 16604–44
[47] Yang Y, Wu J, Xu X, Liang Y, Chu S T, Little B E, Morandotti R, Jia B and Moss D J 2018 Invited article: enhanced four-wave mixing in waveguides integrated with graphene oxide *APL Photonics* **3** 120803
[48] Boyraz O, Koonath P, Raghunathan V and Jalali B 2004 All optical switching and continuum generation in silicon waveguides *Opt. Express* **12** 4094–102
[49] Marini A, Cox J D, García F J Abajo D 2017 Theory of graphene saturable absorption *Phys. Rev.* B **95** 125408
[50] Baudisch M *et al* 2018 Ultrafast nonlinear optical response of Dirac fermions in graphene *Nat. Commun.* **9** 1–6
[51] Bao Q, Zhang H, Wang Y, Ni Z, Yan Y, Shen Z X, Loh K P and Tang D Y 2009 Atomic-layer graphene as a saturable absorber for ultrafast pulsed lasers *Adv. Funct. Mater.* **19** 3077–83
[52] Oskooi A F, Roundy D, Ibanescu M, Bermel P, Joannopoulos J D and Johnson S G 2010 Meep: a flexible free-software package for electromagnetic simulations by the FDTD method *Comput. Phys. Commun.* **181** 687–702
[53] Krückel C J *et al* 2017 Optical bandgap engineering in nonlinear silicon nitride waveguides *Opt. Express* **25** 15370–80
[54] Kitamura R, Pilon L and Jonasz M 2007 Optical constants of silica glass from extreme ultraviolet to far infrared at near room temperature *Appl. Opt.* **46** 8118–33
[55] Serkin V N and Vysloukh V A 1993 Blue self-frequency shift of femtosecond optical solitons *Nonlinear Guided Wave Phenomena, Technical Digest* vol 15 (Optical Society of America)
[56] Hölzer P, Chang W, Travers J, Nazarkin A, Nold J, Joly N, Saleh M F, Biancalana F and Russell P S J 2011 Femtosecond nonlinear fiber optics in the ionization regime *Phys. Rev. Lett.* **107** 203901
[57] Saleh M F, Chang W, Hölzer P, Nazarkin A, Travers J C, Joly N Y, Russell P S J and Biancalana F 2011 Theory of photoionization-induced blueshift of ultrashort solitons in gas-filled hollow-core photonic crystal fibers *Phys. Rev. Lett.* **107** 203902
[58] Monat C, Corcoran B, Ebnali-Heidari M, Grillet C, Eggleton B J, White T P, O'Faolain L and Krauss T F 2009 Slow light enhancement of nonlinear effects in silicon engineered photonic crystal waveguides *Opt. Express* **17** 2944–53
[59] Roy S, Marini A and Biancalana F 2013 Self-frequency blueshift of dissipative solitons in silicon-based waveguides *Phys. Rev.* A **87** 065803